

# **$^{89}\text{Zr}$ Labeled Anti-PD-L1 Antibody PET Monitors Gemcitabine Therapy-Induced Modulation of Tumor PD-L1 Expression**

**(Short title: Imaging Therapeutic Modulation of PD-L1)**

Kyung-Ho Jung<sup>1,2\*</sup>, Jin Won Park<sup>3</sup>, Jin Hee Lee<sup>1,2</sup>,  
Seung Hwan Moon<sup>1</sup>, Young Seok Cho<sup>1</sup>, Kyung-Han Lee<sup>1,2</sup>

<sup>1</sup>Department of Nuclear Medicine, Samsung Medical Center and <sup>2</sup>Samsung Advanced Institute for Health Sciences & Technology, Sungkyunkwan University School of Medicine, Seoul, Korea, <sup>3</sup>Scripps Korea Antibody Institute, Chuncheon-si, Gangwon-do, Korea

Corresponding Author: Kyung-Han Lee, MD, PhD,  
Samsung Medical Center, 50 Ilwon-dong, Gangnam-gu, Seoul, Korea.  
Tel: 82-2-3410-2630; fax: 82-2-3410-2639; [khleenm@naver.com](mailto:khleenm@naver.com)

First Author: Kyung-Ho Jung, PhD.

Address, same as above

Tel: 82-2-3410-2649; fax: 82-2-3410-2639; [jkhope0834@gmail.com](mailto:jkhope0834@gmail.com)

This research was supported by Basic Science Research Program through the National Research Foundation of Korea (NRF) funded by the Ministry of Education (2016R1D1A1B03932202) and the NRF grant funded by the Korean government (MIST) (2019R1A2C1084959).

**Key words:**  $^{89}\text{Zr}$ , PD-L1, antibody, cancer, gemcitabine, immuno-PET

## ABSTRACT

We developed an  $^{89}\text{Zr}$ -labeled anti-programmed death ligand 1 (anti-PD-L1) immune PET that can monitor chemotherapy-mediated modulation of tumor PD-L1 expression in living subjects. **Methods:** Anti-PD-L1 underwent sulfhydryl moiety-specific conjugation with maleimide-deferoxamine followed by  $^{89}\text{Zr}$  radiolabeling. CT26 colon cancer cells and PD-L1 overexpressing CT26/PD-L1 cells underwent binding assays, flow cytometry, and Western blotting. In vivo pharmacokinetics, biodistribution, and PET imaging was evaluated in mice. **Results:**  $^{89}\text{Zr}$ -anti-PD-L1 synthesis was straightforward and efficient. SDS PAGE showed that reduction produced half-antibody fragments, and MALDI-TOF analysis estimated 2.18 conjugations per antibody, indicating specific conjugation at the hinge region disulfide bonds. CT26/PD-L1 cells showed  $102.2 \pm 6.7$ -fold greater  $^{89}\text{Zr}$ -anti-PD-L1 binding compared to weak expressing CT26 cells. Excellent target specificity was confirmed by a drastic reduction of binding by excess cold antibody. Intravenous  $^{89}\text{Zr}$ -anti-PD-L1 followed bi-exponential blood clearance. PET/CT image analysis demonstrated decreases in major organ activity over 7 days, whereas high CT26/PD-L1 tumor activity was maintained. Again, this was suppressed by excess cold antibody. Treatment of CT26 cells with gemcitabine for 24 h augmented PD-L1 protein to  $592.4 \pm 114.2\%$  of controls and increased  $^{89}\text{Zr}$ -anti-PD-L1 binding. This was accompanied by increased AKT activation and reduced PTEN. In CT26 tumor-bearing mice, gemcitabine treatment substantially increased tumor uptake from  $1.56 \pm 0.48$  to  $6.24 \pm 0.37$  %ID/g (tumor/blood ratio: 34.7). Immunoblots revealed significant increases in tumor PD-L1 and activated AKT and a decrease of PTEN. **Conclusion:**  $^{89}\text{Zr}$ -anti-PD-L1 showed specific targeting with favorable imaging properties. Gemcitabine treatment upregulated cancer cell and tumor PD-L1 expression and increased  $^{89}\text{Zr}$ -anti-PD-L1 uptake.  $^{89}\text{Zr}$ -anti-PD-L1 PET may thus be useful for monitoring chemotherapy-mediated tumor PD-L1 modulation in living subjects.

## INTRODUCTION

Immune checkpoint therapy is revolutionizing treatment of cancers that evade immune surveillance, and PD-L1 stands out as a promising target (1). This transmembrane protein engages with PD-1 on T cells to suppress their proliferation, survival, and cytokine production (2). Accordingly, inhibitors that block PD-1/PD-L1 interaction show antitumor effects (1). However, treatment benefit remains limited to only a fraction of cancer patients.

The first obvious question for predicting a PD-L1 blockade response is whether the target protein is sufficiently present (3). Immunohistochemistry of biopsied specimen is limited by inter- and intra-lesion heterogeneities (4) and is unable to assess whole tumor PD-L1 amount that may influence immunotherapy efficacy (5). Positron emission tomography (PET) can overcome limitations of immunohistochemistry including sampling error, invasiveness, and difficulty of serial examinations (6). Immuno-PET has thus been demonstrated to detect tumor PD-L1 with high sensitivity and resolution (7,8).

It is also critical to recognize that tumor PD-L1 status changes over time (9). This dynamic nature of expression might contribute to varied therapeutic responses, which underscores the importance of better understanding tumor PD-L1 regulation (10). In addition to transcriptional regulation by inflammatory signaling (11), there is rising interest in the influence of chemotherapeutic agents (12-15). Given the current clinical trials combining immunotherapy with conventional chemotherapeutics (16), the ability to monitor the immuno-modulatory effects of chemotherapeutic drugs will benefit their rational use. However, current investigations are limited by their dependence on peripheral blood (17) rather than tumor PD-L1 status. Assessment of changes in the immunological status of the tumor by chemotherapeutics may be provided by immune PET.

In this study, we developed an antibody site-specifically labeled with  $^{89}\text{Zr}$  that allows high resolution and specific imaging of tumor PD-L1. We then explored the capacity of this radiotracer to noninvasively monitor changes of PD-L1 expression on cancer cells and tumors before and after treatment with gemcitabine. We further explored the signaling pathways that are involved.

## **MATERIALS AND METHODS**

### **Cell Culture and Reagents**

CT26 mouse colon cancer cells (American Type Culture Collection) were maintained in 5% CO<sub>2</sub> at 37°C in RPMI 1640 supplemented with 10% fetal bovine serum (FBS), 2 mM L-glutamine, and 100 U/ml penicillin-streptomycin. Gemcitabine, olaparib, 5-fluorouracil (5-FU), cisplatin, and MHY1485 were from Sigma Chemicals. Rapamycin was from LC Laboratories.

### **Preparation of Cells Stably Overexpressing PD-L1**

We used a Cd274 (NM\_021893) mouse tagged ORF clone lentiviral particle from Origene. The lentiviral particle was constructed with the pLenti-C-mGFP-P2A-Puro Tagged Cloning Vector that contains mGFP gene and puromycin resistance gene as selection markers. PD-L1 overexpressing CT26/PD-L1 cells were prepared by infection with the lentivirus followed by selection 72 h later under 10 µg/ml puromycin. Single-cell clones were picked up, amplified in media containing puromycin, and stored in liquid nitrogen. The clone with greatest specific anti-PD-L1 binding was used.

### **Deferoxamine Conjugation and Site-Specific <sup>89</sup>Zr Labeling**

Rat IgG against mouse PD-L1 (10F.9G2; BioXcell, West Lebanon, NH) was site-specifically conjugated with deferoxamine-maleimide on sulfhydryl residues. Briefly, 2 mg of antibody were incubated with 100 mM tris(2-carboxyethyl)phosphine (TCEP) for 20 min at room temperature (RT) at a 1:100 molar ratio. Sulfhydryl residues of anti-PD-L1 diluted in 0.1 M sodium phosphate containing 150 mM NaCl and 1 mM EDTA were conjugated for 60 min at RT with 56.4 µl of 2mM N-(3,11,14,22,25,33-hexaoxo-4,10,15,21,26,32-hexaaza-10,21,32-trihydroxytetratriacontane) maleimide (deferoxamine-maleimide). The molar ratio of deferoxamine-maleimide to antibody that was 60:1. <sup>89</sup>Zr-oxalate (50 µl; Korea Atomic Energy Research Institute) was neutralized with 25 µl of 2 M Na<sub>2</sub>CO<sub>3</sub> and mixed with deferoxamine-conjugated anti-PD-L1 in 75 µl of 0.5 M HEPES buffer (pH 7.5). Following 60 min of

incubation at RT, the mixture was eluted through a PD-10 column with 0.25 M sodium acetate containing 0.5% gentisic acid. Fractions of 0.5 ml were collected, counted for radioactivity, and the peak activity fraction was used.

### **Matrix-Assisted Laser Desorption Ionization (MALDI)-TOF**

Intact and deferoxamine-conjugated (by TCEP reduction) anti-PD-L1 was analyzed by mass spectrometry. Samples mixed (1:1 v/v) with sinapinic acid matrix solution (10 mg/ml) were prepared in 50% acetonitrile and 0.1% trifluoroacetic acid, and 1  $\mu$ l was deposited and air dried on a ground stainless steel 384-density MALDI plate. Zip tips were used to desalt the samples. MALDI mass spectra and tandem mass spectra were acquired using a MALDI-TOF 5800 System (AB SCIEX) with a linear mode and an accelerating voltage of 25 kV.

### **Polyacrylamide Gel Electrophoresis (PAGE) and Autoradiography**

For non-reducing sodium dodecyl sulfate (SDS) PAGE, 2  $\mu$ g of antibody samples were diluted with water and 5x non-reducing sample buffer without dithiothreitol. Samples were boiled at 95°C for 10 min, then separated on an 8% SDS PAGE gel by electrophoresis. The gel was stained with 0.5% Coomassie blue. Autoradiography was also performed for  $^{89}\text{Zr}$ -anti-PD-L1, which was separated by 8% native PAGE with sample buffer without SDS or dithiothreitol.

### **Radiochemical Purity and Stability**

Radiochemical purity and stability were assessed by radio-instant thin layer chromatography (radio-iTLC). The radiotracer was incubated in FBS or phosphate buffered saline (PBS) at 37 °C for 0, 1 or 4 days. Radio-TLC was then performed using 50 mM ethylene diamine tetraacetic acid (EDTA, pH 5.5) as eluent on an iTLC-SG glass microfiber chromatography paper impregnated with silica gel. Under this condition, intact radiolabeled antibody remains at baseline while free  $^{89}\text{Zr}^{4+}$  ions and  $^{89}\text{Zr}$ -EDTA migrate at the solvent front.

### **Cell Binding Assays**

CT26 and CT26/PD-L1 cells were incubated with 74 kBq of <sup>89</sup>Zr-anti-PD-L1 for 60 min at 37 °C in RPMI 1640. Cells were washed twice with cold PBS, lysed with 0.5 ml 0.1 N NaOH, and measured for radioactivity. Binding specificity was evaluated with 100 nM cold anti-PD-L1.

### **Flow Cytometry for PD-L1 Expression**

Cell surface-expressed PD-L1 was assessed by flow cytometry using a phycoerythrin (PE)-conjugated antibody against PD-L1 (Clone MIH5). Cells were harvested with non-enzymatic cell-dissociation solution, washed, and incubated with the PE antibody for 30 min at RT in PBS containing 5% FBS and 0.2% bovine serum albumin. After washing with FACS buffer, 500 µl FACS buffer was added and flow cytometry was performed on a FACS Calibur using CellQuest software.

### **Immunohistochemistry for Tumor PD-L1 Expression**

Frozen tumor sections underwent overnight incubation at 4°C with a primary anti-mouse PD-L1 antibody (Abcam, #ab213480; 1:200). An EnVision™ Detection System kit (peroxidase-conjugated polymer backbone, DAKO) was used to incubate slides with anti-rabbit secondary antibody. Finally, sections were counterstained with hematoxylin and mounted with coverslips.

### **Western Blotting of Cultured Cell and Tumor Tissue Protein**

Immunoblotting was performed as previously described (18). Overnight incubation was performed at 4°C with rabbit primary antibodies against PD-L1 (Abcam, ab213480; 1:1000) and phosphorylated forms of AKT (p-AKT) (Cell Signaling Technology, #4058S; 1:1000), mammalian target of rapamycin (p-mTOR) (#2971S; 1:2000), and phosphatase and tensin homolog (p-PTEN) (#9549S; 1:1000). After washing with TBST buffer, membranes were incubated with HRP-conjugated secondary anti-rabbit IgG antibodies (Santa Cruz Biotechnology, 7074S; 1:2000 or 1:4000) at RT for 1 h. Immunoreactive protein was detected with enhanced chemiluminescence substrate and band intensities were quantified as

previously described. After visualizing target protein, membranes were stripped and re-incubated with antibodies against  $\beta$ -actin (Santa Cruz Biotechnology, sc47778), total forms of AKT (t-AKT) (Cell Signaling Technology, #9272S), t-mTOR (#2972S), or t-PTEN (#9552S).

### **In Vivo Pharmacokinetics**

All animal experiments were conducted in accordance with the National Institute of Health Guide for the Care and Use of Laboratory Animals and approved by the Institute ethics committee. For pharmacokinetic analysis, normal C57BL/6 mice were intravenously injected with 3 MBq  $^{89}\text{Zr}$ -anti-PD-L1. Serially collected blood from the tail vein (5  $\mu\text{l}$ ) were measured for radioactivity and expressed as % injected dose (%ID) per ml. Time activity curves were fitted by non-linear regression with GraphPad Prism V3.02 using two-phase exponential decay equations. Early and late clearance rate constants (K1 and K2) and half-lives ( $T_{1/2\alpha}$  and  $T_{1/2\beta}$ ) were calculated as parameters.

### **Murine Tumor Models and Gemcitabine Treatment**

Tumor models were prepared in Balb/c mice by subcutaneous injection of  $5 \times 10^6$  CT26 or CT26/PD-L1 cells into the right shoulder. When tumor diameter reached 0.5 cm at approximately 10 days after cell inoculation, biodistribution and PET imaging was performed with or without cold anti-PD-L1 blocking.

The effect of gemcitabine was investigated in CT26 tumor-bearing mice. Randomly allocated control and gemcitabine groups were intraperitoneally injected with DMSO vehicle and 100 mg/kg gemcitabine, respectively, every 3-days for three times.

### **In Vivo PET Imaging and Biodistribution Studies in Tumor Models**

Mice intravenously injected with 4.8 MBq  $^{89}\text{Zr}$ -anti-PD-L1 were isoflurane anesthetized and underwent PET/CT on a Siemens Inveon scanner. Specificity of uptake was assessed by 1 h pre-injection of a 5:1 molar ratio of cold anti-PD-L1 antibody over the radiotracer. PET-based tissue radioactivity was measured on non-attenuation corrected coronal images by placing regions-of-interest (ROIs) on the blood

pool, major organs, and tumor. Tumor margins were automatically delineated using a 50% threshold of maximal activity to include the entire tumor while excluding normal tissue. After PET/CT imaging, mice were sacrificed by cervical dislocation, and major organs and tumors were extracted, weighed, and measured for radioactivity.

### **Statistical Analysis**

Data are presented as means  $\pm$  SD unless otherwise specified. Significant differences between groups were analyzed by two-tailed unpaired Student's t-tests for two groups and ANOVA with Tukey's post-hoc test for three or more groups. *P* values less than 0.05 were statistically significant.

## RESULTS

### DFO-conjugation and Site-Specific <sup>89</sup>Zr Labeling

B7-H1 anti-PD-L1 was conjugated on sulfhydryl residues (Fig. 1A). Non-reduced SDS-PAGE demonstrated that TCEP completely reduced target disulfide bonds to produce fragments half the size of the intact antibody, which remained reduced after DFO-conjugation (Fig. 1A). The MALDI peak measured by mass spectrometry revealed a mass of 147786.83 Da for unmodified antibody and 75443.23 Da for DFO-conjugated antibody (Fig. 1A). This indicates an average of 2.18 conjugations per antibody that likely corresponds to the two hinge region disulfide bonds.

<sup>89</sup>Zr labeling was reproducible with an efficiency of > 80% (Fig. 1B). PAGE analysis of the first peak elute fraction displayed a clear radioactive band at the 170 kD region (Fig. 1B). Radiochemical purity was > 99%, and specific activity was 0.8 mCi/mg. Radiochemical stability by iTLC showed that the radiolabel was > 96% intact after 96 h incubation in 50% FBS as well as in PBS (Fig. 1B).

### Cancer Cell Binding

Compared to parental CT26 cells, CT26/PD-L1 cells displayed  $7.5 \pm 0.4$ -fold higher levels of PD-L1 protein (Fig. 2A). Cell binding assays revealed high <sup>89</sup>Zr-anti-PD-L1 binding to CT26/PD-L1 cells that reached 100.2-fold of binding to CT26 cells. This was completely abolished to  $3.0 \pm 0.8\%$  of the unblocked level by 100 nM cold anti-PD-L1 (Fig. 2A).

### In Vivo Pharmacokinetic Properties

In normal mice, intravenous <sup>89</sup>Zr-anti-PD-L1 followed a bi-exponential pattern of blood clearance. Early K1 and late K2 rate constants of 0.11 and 0.0189 led to an early distribution half-life ( $T_{1/2\alpha}$ ) of 6.3 h and late clearance half-life ( $T_{1/2\beta}$ ) of 36.7 h (Fig. 2B). ROI analysis of PET/CT images in CT26/PD-L1 tumor mice showed that whereas blood pool, lung, liver, and muscle activity decreased over time, tumor activity was maintained at a high level for up to 7 days (Fig. 2B). Hence, 7-days post-injection was

selected for the remainder of experiments.

### **Tissue Biodistribution and PET Imaging**

Biodistribution on day 7 revealed high  $^{89}\text{Zr}$ -anti-PD-L1 accumulation in CT26/PD-L1 tumors that reached  $12.6 \pm 5.1$  %ID/g, which was 3.9-fold of CT26 tumors. Pre-injection of cold anti-PD-L1 caused a 66.1% reduction in CT26/PD-L1 tumor uptake, confirming specific uptake (Fig. 3A). Remarkably, liver, spleen and renal activities were relatively low.

PET/CT imaging displayed clear tumor visualization from 4 days (Fig. 3B). Again, there was relatively low uptake in the liver, spleen, and kidneys. Image-based CT26/PD-L1 tumor uptake slightly increased from day 4 to day 7, whereas uptake in CT26 tumors slightly decreased (Fig. 3B). CT26/PD-L1 tumor uptake was significantly reduced by cold anti-PD-L1.

### **Chemotherapy Induces PD-L1 Expression on Cancer Cells**

$^{89}\text{Zr}$ -anti-PD-L1 binding to CT26 cells was CDDP dose-dependently increased to  $179.1 \pm 38.0\%$  of controls by 24 h treatment and was further increased to  $247.6 \pm 55.1\%$  when 500  $\mu\text{M}$  5-FU was combined. Binding was increased by 10  $\mu\text{M}$  olaparib to  $145.1 \pm 2.2\%$  of controls (Fig. 4A).

Immunoblotting revealed that CT26 cell PD-L1 expression was substantially increased to  $592.4 \pm 114.2\%$  and  $224.8 \pm 155.9\%$  of controls by 50 nM gemcitabine and 10  $\mu\text{M}$  olaparib, respectively (Fig. 4B). FACS analysis confirmed that 24 h gemcitabine treatment increased PD-L1 positive CT26 cells from  $11.3 \pm 0.9\%$  at baseline to  $46.6 \pm 1.0\%$  (Fig. 4B). Gemcitabine treatment at 500 nM increased  $^{89}\text{Zr}$ -anti-PD-L1 binding to  $145.4 \pm 7.8\%$  of controls (Fig. 4B).

### **Roles of AKT and PTEN Signaling**

Western blot analysis showed that 500 nM gemcitabine substantially increased CT26 cell PD-L1 protein to  $799.9 \pm 70.1\%$  of controls ( $P < 0.005$ ). Among potential signaling proteins, gemcitabine-treatment increased p-AKT to  $184.3 \pm 17.0\%$  ( $P < 0.05$ ) and reduced p-PTEN to  $53.4 \pm 0.6\%$  of controls

( $P < 0.001$ ; Fig. 5A). PD-L1 expression stimulated by gemcitabine was modestly augmented from  $451.0 \pm 13.6\%$  to  $502.8 \pm 15.5\%$  of controls ( $P = 0.07$ ) by the mTOR inhibitor rapamycin, while it was suppressed to  $372.9 \pm 0.8\%$  of controls ( $P = 0.015$ ) by the specific mTOR activator MHY1485 (Fig. 5B). Together, these results demonstrate roles for AKT activation and reduced PTEN activation in the ability of gemcitabine to upregulate PD-L1, and further suggest a role for mTOR signaling.

### **In Vivo Effects of Gemcitabine on Tumors**

In murine models, gemcitabine substantially enhanced CT26 tumor  $^{89}\text{Zr}$ -anti-PD-L1 uptake at 7 days to  $6.24 \pm 0.37\% \text{ID/g}$ , compared to only  $1.56 \pm 0.48\% \text{ID/g}$  in controls ( $P < 0.005$ ; Fig. 6A). Tumor-to-blood ratio was  $38.2 \pm 11.3$  and  $11.9 \pm 2.78$  for gemcitabine and control groups, respectively (data not shown). PET/CT recapitulated these findings by showing significantly higher CT26 tumor uptake ( $8.5 \pm 0.14$  vs.  $5.15 \pm 0.78\% \text{ID/g}$ ,  $P < 0.05$ ) and tumor-to-tissue ratios after gemcitabine treatment (Fig. 6B).

Immunohistochemistry confirmed strong PD-L1 staining in CT26 tumor tissue from gemcitabine-treated mice, but weak staining in controls (Fig. 7A). Finally, CT26 tumor tissues revealed that PD-L1 expression ( $P < 0.05$ ) and AKT activation ( $P < 0.005$ ) were significantly increased following gemcitabine treatment, whereas PTEN expression was significantly suppressed, ( $P < 0.001$ ; Fig. 7B).

## DISCUSSION

In this study, we developed an immune-PET that can noninvasively image tumor PD-L1 status. The monoclonal antibody used was a rat IgG2b (10F.9G2) that specifically binds to the extracellular domain of mouse PD-L1. Although rat antibodies are limited in use for clinical translation, the 10F.9G2 antibody has been used in several previous studies to investigate PD-L1 expression and function (19-21). The antibody has been shown to block PD-L1/PD-1 interaction and is used for Western blotting, immunochemistry, FACS, and as a neutralizing antibody. High affinity for PD-L1 comparable to 10F.2H11 antibody (20) and binding specific for PD-L1 was shown (21).

<sup>89</sup>Zr-anti-PD-L1 showed prominent binding to cancer cells with high PD-L1 expression and had high target specificity, indicating good immuno-reactivity. Cysteine-specific conjugation is an elegant way of tailoring the location of <sup>89</sup>Zr attachment to antibodies for PET (22). The maleimide-deferoxamine conjugation technique we exploited has not been reported for <sup>89</sup>Zr labeling of anti-PD-L1, although it has been utilized for other antibodies. A very recent study successfully conjugated anti-PD-L1 to deferoxamine chelators site-specifically on enzymatically modified glycans prior to <sup>89</sup>Zr labeling (8). However, this procedure required overnight reaction at 37 °C, whereas our method was straightforward and efficient with a short 1-h reaction at RT.

Our analysis indicated that TCEP treatment led to site-specific reduction and DFO-conjugation of our antibody, likely at the two hinge region disulfide bonds. This is consistent with the notion that preferential reduction of the hinge region disulfide bonds yields monovalent components with free thiol groups that can be employed for site-directed labeling (23). Site-specific conjugation allows radioprobe homogeneity and immuno-reactivity compared to other nonspecific radiolabeling methods, and its advantages for in vivo imaging are well-established.

<sup>89</sup>Zr-anti-PD-L1 PET visualized CT26/PD-L1 tumors with excellent contrast by 4-days post-injection. Accumulation was high in overexpressing CT26/PD-L1 tumors but low in weakly expressing CT26

tumors. Previous studies with  $^{89}\text{Zr}$  labeled antibodies against PD-L1 have shown high splenic uptake, which is attributed to PD-L1 expressing splenic cells. At low tracer doses, the spleen acts as a sink organ that reduces tumor targeting (23). Our radiotracer showed low liver and renal uptake, which is an advantage for imaging intra-abdominal tumors. Spleen uptake was also only modest, likely because we injected a relatively higher radiotracer dose to reduce splenic accumulation. Indeed, it is known that increasing tracer dose can saturate spleen uptake and restore tumor targeting (24).

Because only a small portion of patients respond to checkpoint inhibitors as monotherapy, there is growing interest in combining other chemotherapies to enhance treatment efficacy (16). Each chemotherapeutic drug impacts the tumor microenvironment differently, and selection of the best combination partner requires a better understanding of these behaviors. This study attempted to monitor this effect using PD-L1 targeted immune PET. We tested the effects of the pyrimidine nucleoside analogue gemcitabine. Previous studies showed that gemcitabine shows anti-tumor activities in a manner less related to drug sensitivity but rather correlated with the immunogenicity of the tumor (25). Preclinical studies using gemcitabine combined with immune checkpoint inhibitors have shown tumor control and survival that outperformed immunotherapy alone (14).

In our results, gemcitabine increased  $^{89}\text{Zr}$ -anti-PD-L1 binding to cancer cells in vitro and uptake in tumors in vivo. In mice, gemcitabine-stimulated uptake was restricted to the tumor, while uptake in other organs including the spleen was unaffected. This was attributed to upregulated PD-L1 levels. Upregulated tumor PD-L1 expression by gemcitabine was previously observed in other cancer types (13,15). This represents an opportunity for inducing a more effective response to immune checkpoint blockade.

Mechanistically, chemotherapeutic drugs might modulate PD-L1 expression in cancer cells through oncogenic signaling. In hepatoma cells, cisplatin-induced PD-L1 upregulation was shown to occur through ERK1/2 activation (12). Another study on pancreatic cancer cells suggested that 5-FU, paclitaxel, or high dose gemcitabine increased PD-L1 expression through JAK/STAT signaling (13). In our study,

cultured CT26 cells and CT26 tumors showed reduction of the tumor-suppressor PTEN following gemcitabine treatment. PTEN alterations are thought to contribute to tumor escape from PD-1/PD-L1 inhibition (26). Previous studies showed that PTEN loss in malignant cells increased PD-L1 expression (27-29). This supports the role of PTEN reduction in the strengthening of tumor PD-L1 expression by gemcitabine.

PTEN is a major negative regulator of AKT signaling (22), and PTEN reduction in tumors is associated with AKT activation (29,30). In our results, gemcitabine-treated CT26 cells and CT26 tumors displayed increased AKT activation accompanying PD-L1 upregulation. Therapeutic AKT targeting is recognized to enhance immune surveillance (31), and early clinical efficacy has been demonstrated. In addition, AKT signaling has been implicated to upregulate cancer PD-L1 expression (30). In glioma cells, AKT activation by PTEN loss increased PD-L1 expression (27). In colon cancer cells, PTEN loss strengthened and pharmacological AKT inhibition suppressed PD-L1 expression (29). Taken together, the stimulation of PD-L1 expression by gemcitabine could be explained by PTEN reduction that caused AKT activation. This supports the benefit of combining drugs that target oncogenic PTEN and AKT pathways to improve the outcome of immune checkpoint therapies.

Although it would be interesting to explore whether gemcitabine can lead to better efficacy of anti-PD-L1 therapy, the antitumor effect of gemcitabine itself would require adjusting drug dose and timing with a large number of animals. Therefore, this experiment was beyond the scope of the present study.

Our results suggest that  $^{89}\text{Zr}$ -anti-PD-L1 PET could be used in screening for drugs to combine with immune checkpoint therapies. Inducible tumor PD-L1 expression is likely transient rather than persistent (15), and the impact of drug dosage on immunomodulatory effects has yet to be elucidated. Therefore,  $^{89}\text{Zr}$ -anti-PD-L1 PET may be helpful for selecting the optimal combination treatment protocol including timing, dosage, and sequence of administration for best patient outcomes.

## CONCLUSION

Gemcitabine increased CT26 cell PD-L1 expression, and this was faithfully represented by augmented cellular  $^{89}\text{Zr}$ -anti-PD-L1 binding in vitro and tumor uptake in vivo. Thus,  $^{89}\text{Zr}$ -anti-PD-L1 PET may be useful for noninvasively monitoring PD-L1 modulation to screen for conventional drugs that can enhance the efficacy of immune checkpoint therapies.

## DISCLOSURE

No potential conflict of interest relevant to this article was reported.

## KEY POINTS

- **QUESTION:** Can immune PET based noninvasively monitor changes in tumor PD-L1 expression induced by conventional chemotherapy?
- **PERTINENT FINDINGS:**  $^{89}\text{Zr}$ -anti-PD-L1 showed PD-L1-dependent specific binding to CT26 cancer cells and provided high contrast tumor imaging. Gemcitabine increased CT26 cell PD-L1 expression, and this was faithfully represented by augmented cellular binding of  $^{89}\text{Zr}$ -anti-PD-L1 in vitro and tumor uptake in vivo.
- **IMPLICATIONS FOR PATIENT CARE:**  $^{89}\text{Zr}$ -anti-PD-L1 PET may be useful for noninvasively monitoring PD-L1 modulation to screen for conventional drugs that can enhance the efficacy of immune checkpoint therapies.

## REFERENCES

1. Topalian SL, Hodi FS, Brahmer JR, et al. Safety, activity, and immune correlates of anti-PD-1 antibody in cancer. *N Engl J Med.* 2012;366:2443-2454.
2. Butte MJ, Keir ME, Phamduy TB, Sharpe AH, Freeman GJ. Programmed death-1 ligand 1 interacts specifically with the B7-1 costimulatory molecule to inhibit T cell responses. *Immunity.* 2007;27:111-122.
3. Song Y, Li Z, Xue W, Zhang M. Predictive biomarkers for PD-1 and PD-L1 immune checkpoint blockade therapy. *Immunotherapy.* 2019;11(6):515-529.
4. McLaughlin J, Han G, Schalper KA, et al. Quantitative assessment of the heterogeneity of PD-L1 expression in non-small-cell lung cancer. *JAMA Oncol.* 2016;2:46-54.
5. Brodská B, Otevřelová P, Šálek C, Fuchs O, Gašová Z, Kuželová K. High PD-L1 expression predicts for worse outcome of leukemia patients with concomitant NPM1 and FLT3 mutations. *Int J Mol Sci.* 2019;20:2823.
6. Meng Y, Sun J, Qv N, Zhang G, Yu T, Piao H. Application of molecular imaging technology in tumor immunotherapy. *Cell Immunol.* 2020;348:104039.
7. Bensch F, van der Veen EL, Lub-de Hooge MN, et al. <sup>89</sup>Zr-artezolizumab imaging as a non-invasive approach to assess clinical response to PD-L1 blockade in cancer. *Nat Med.* 2018;24:1852-1858.
8. Christensen C, Kristensen LK, Alfsen MZ, Nielsen CH, Kjaer A. Quantitative PET imaging of PD-L1 expression in xenograft and syngeneic tumour models using a site-specifically labelled PD-L1 antibody. *Eur J Nucl Med Mol Imaging.* 2020;47:1302-1313.
9. Guan J, Wang R, Hasan S, et al. Prognostic significance of the dynamic change of programmed death-ligand 1 expression in patients with multiple myeloma. *Cureus.* 2019;11(4):e4401.
10. Sun C, Mezzadra R, Schumacher TN. Regulation and function of the PD-L1 checkpoint. *Immunity.* 2018;48:434-452.

11. Dong H, Strome SE, Salomao DR, et al. Tumor-associated B7-H1 promotes T-cell apoptosis: a potential mechanism of immune evasion. *Nat Med.* 2002;8:793-800.
12. Qin X, Liu C, Zhou Y, Wang G. Cisplatin induces programmed death-1-ligand (PD-L1) overexpression in hepatoma H22 cells via Erk/MAPK signaling pathway. *Cell Mol Biol.* 2010;56:OL1366-1372.
13. Doi T, Ishikawa T, Okayama T, et al. The JAK/STAT pathway is involved in the upregulation of PD-L1 expression in pancreatic cancer cell lines. *Oncol Rep.* 2017;37:1545-1554.
14. Tallón de Lara P, Cecconi V, Hiltbrunner S, et al. Gemcitabine synergizes with immune checkpoint inhibitors and overcomes resistance in a preclinical model and mesothelioma patients. *Clin Cancer Res.* 2018;24:6345-6354.
15. Peng J, Hamanishi J, Matsumura N, et al. Chemotherapy induces programmed cell death-ligand 1 overexpression via the nuclear factor- $\kappa$ B to foster an immunosuppressive tumor microenvironment in ovarian cancer. *Cancer Res.* 2015;75:5034-5045.
16. Smyth MJ, Ngiew SF, Ribas A, Teng MW. Combination cancer immunotherapies tailored to the tumour microenvironment. *Nat Rev Clin Oncol.* 2016;13:143-158.
17. Homma Y, Taniguchi K, Nakazawa M, et al. Changes in the immune cell population and cell proliferation in peripheral blood after gemcitabine-based chemotherapy for pancreatic cancer. *Clin Transl Oncol.* 2014;16: 330-335.
18. Jung K-H, Lee JH, Park JW, et al. Troglitazone exerts metabolic and antitumor effects on T47D breast cancer cells by suppression mitochondrial pyruvate availability. *Oncol Rep.* 2020;43:711-717.
19. Twyman-Saint Victor C, Rech AJ, Maity A, et al. Radiation and dual checkpoint blockade activate non-redundant immune mechanisms in cancer. *Nature.* 2015;520:373-377.
20. Paterson AM, Brown KE, Keir ME, et al. The PD-L1:B7-1 pathway restrains diabetogenic effector T cells in vivo. *J Immunol.* 2011;187:1097-1105.
21. Eppihimer MJ, Gunn J, Freeman GJ, et al. Expression and regulation of the PD-L1 immunoinhibitory

- molecule on microvascular endothelial cells. *Microcirculation*. 2002;9:133-145.
22. Tinianow JN, Gill HS, Ogasawara A, et al. Site-specifically <sup>89</sup>Zr-labeled monoclonal antibodies for ImmunoPET. *Nucl Med Biol*. 2010;37:289-297.
  23. Makaraviciute A, Jackson CD, Millner PA, Ramanaviciene A. Considerations in producing preferentially reduced half-antibody fragments. *J Immunol Methods*. 2016;429:50-56.
  24. Wierstra P, Sandker G, Aarntzen E, et al. Tracers for non-invasive radionuclide imaging of immune checkpoint expression in cancer. *EJNMMI Radiopharm Chem*. 2019;4:29.
  25. Suzuki E, Sun J, Kapoor V, Jassar AS, Albelda SM. Gemcitabine has significant immunomodulatory activity in murine tumor models independent of its cytotoxic effects. *Cancer Biol Ther*. 2007;6:880-885.
  26. Cretella D, Digiacomo G, Giovannetti E, Cavazzoni A. PTEN alterations as a potential mechanism for tumor cell escape from PD-1/PD-L1 inhibition. *Cancers (Basel)*. 2019;11(9).
  27. Parsa AT, Waldron JS, Panner A, et al. Loss of tumor suppressor PTEN function increases B7-H1 expression and immunoresistance in glioma. *Nat Med*. 2007;13:84-88.
  28. Xu C, Fillmore CM, Koyama S, et al. Loss of LKB1 and PTEN leads to lung squamous cell carcinoma with elevated PD-L1 expression. *Cancer Cell*. 2014;25:590-604.
  29. Song M, Chen D, Lu B, et al. PTEN loss increases PD-L1 protein expression and affects the correlation between PD-L1 expression and clinical parameters in colorectal cancer. *PLoS ONE*. 2013;8(6):e65821.
  30. Atefi M, Avramis E, Lassen A, et al. Effects of MAPK and PI3K pathways on PD-L1 expression in melanoma. *Clin Cancer Res*. 2014;20:3446-3457.
  31. Noh K-H, Kang TH, Kim JH, et al. Activation of Akt as a mechanism for tumor immune evasion, *Mol Ther*. 2009;17:439-447.

**FIGURE 1**

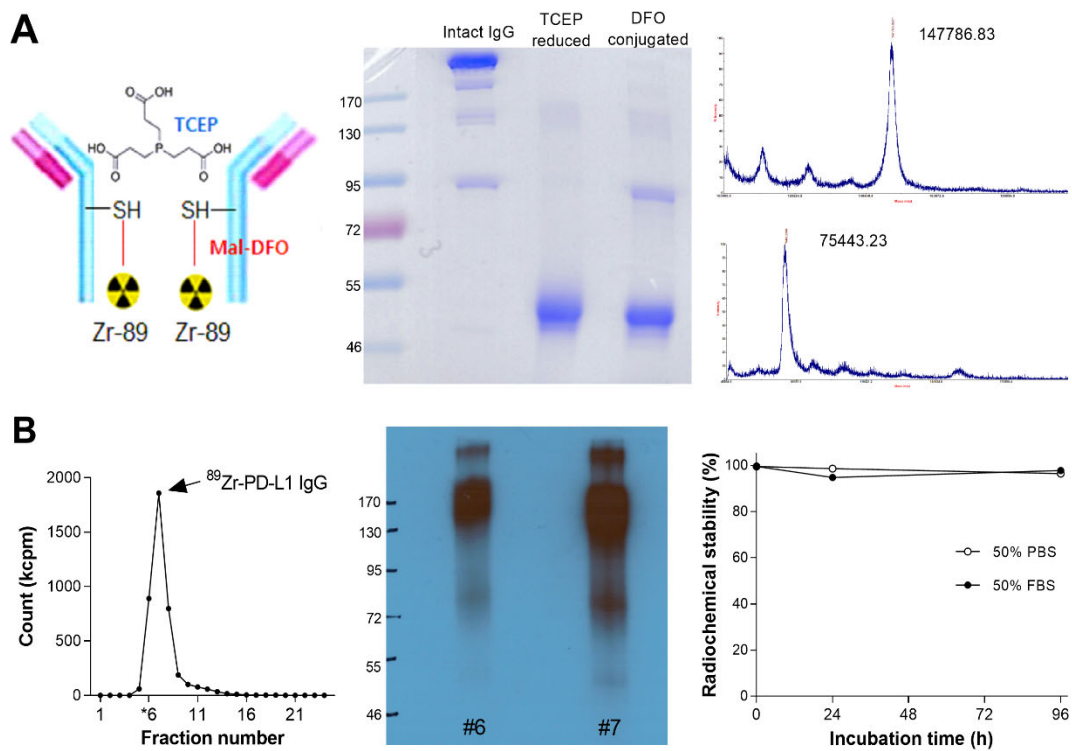


**FIGURE 1.**  $^{89}\text{Zr}$ -labeling of anti-PD-L1. (A) Diagram of  $^{89}\text{Zr}$ -anti-PD-L1 (left), non-reduced SDS PAGE (middle), and MALDI-TOF results (right). (B) Radioactivity profile of PD-10 column-eluted fractions (left), autoradiography on native PAGE (middle), and in vitro stability (right).

**FIGURE 2**

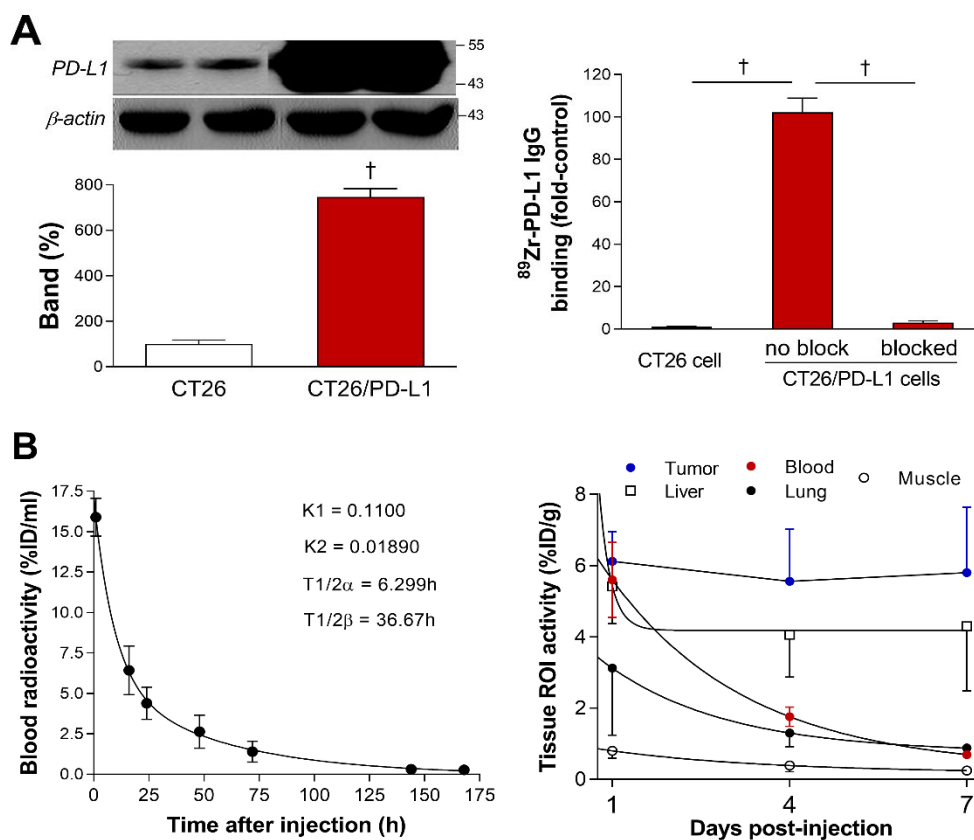


**FIGURE 2.** Cell binding and pharmacokinetic properties. (A) Western blotting of PD-L1 (left) and  $^{89}\text{Zr}$ -anti-PD-L1 binding (right) in CT26 and CT26/PD-L1 cancer cells. Bars are means  $\pm$  S.D.  $\dagger P < 0.005$ . (B) Time-dependent blood clearance (left) in normal mice showing early and late rate constants ( $K1$  and  $K2$ ) and half-lives ( $T1/2\alpha$  and  $T1/2\beta$ ). Pharmacokinetic profile in major organs and tumor measured by PET-based analysis in CT26/PD-L1 tumor mice ( $n = 5$ ) at 1, 4 and 7-days (right).

**FIGURE 3**

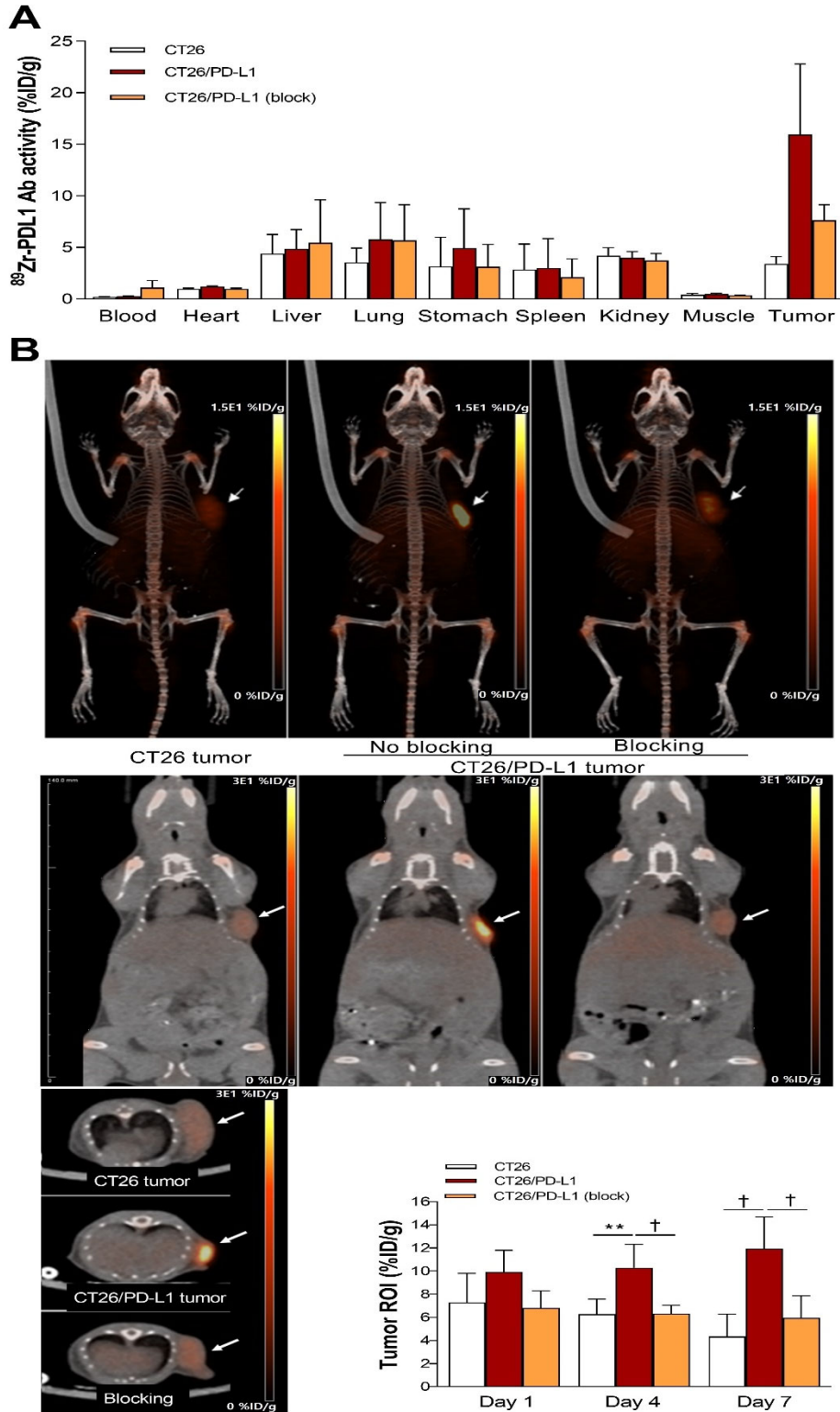


**FIGURE 3.** Biodistribution and tumor imaging. (A) Biodistribution in CT26 and CT26/PD-L1 tumor-bearing mice with or without blocking at day 7. (B) Representative maximum intensity projection (top), coronal (middle), and transaxial (bottom) PET images. PET-based tumor uptakes are also shown. All bars are mean  $\pm$  S.D. of values from 5 mice per group.  $**P < 0.01$ ,  $\dagger P < 0.005$ .

**FIGURE 4**

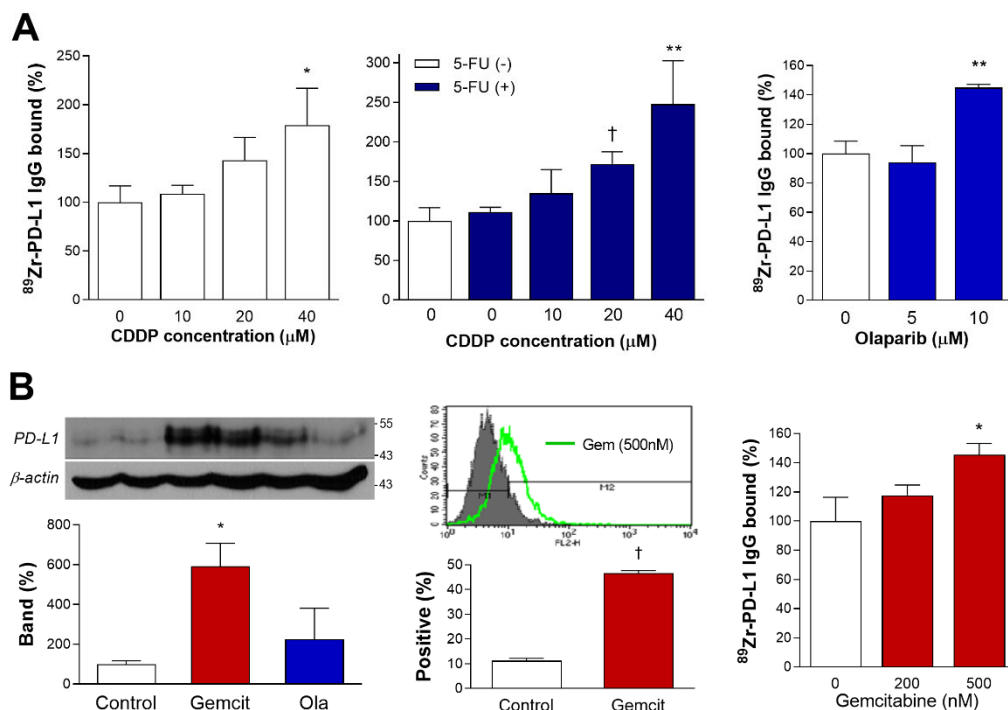


**FIGURE 4.** Effects of chemotherapeutic agents on CT26 cells. (A) Stimulatory effects of 24 h treatment with graded doses of CDDP alone (left), CDDP plus 5-FU (middle), or olaparib (right) on  $^{89}\text{Zr}$ -anti-PD-L1 binding. (B) PD-L1 immunoblots and  $\beta$ -actin-corrected band (left), flow cytometry of PD-L1(+) cells (middle), and  $^{89}\text{Zr}$ -anti-PD-L1 binding (right). Bars are means  $\pm$  S.D. Binding data are from triplicate samples per group. \* $P < 0.05$ , \*\* $P < 0.01$ , and † $P < 0.005$ , compared to controls.

**FIGURE 5**

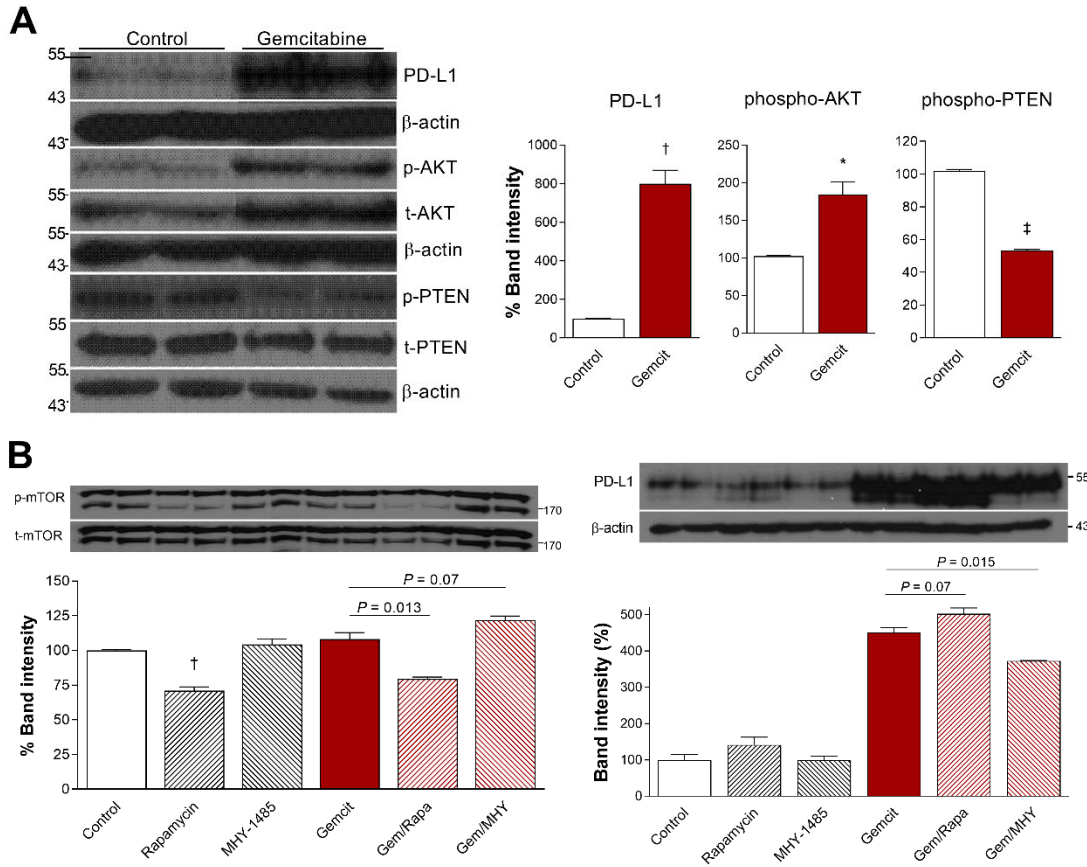


**FIGURE 5.** AKT and PTEN signaling in gemcitabine effect on CT26 cells. (A) Immunoblots and quantified protein band intensities (corrected by appropriate controls) for PD-L1, p-AKT and p-PTEN. (B) Effects of rapamycin (Rapa; 1  $\mu$ M) and MHY1485 (MHY; 2  $\mu$ M) on immunoblots and band intensities for p-mTOR (corrected by t-mTOR) and PD-L1 (corrected by  $\beta$ -actin). Bars are means  $\pm$  S.D. \* $P < 0.05$ ; <sup>†</sup> $P < 0.005$ ; <sup>‡</sup> $P < 0.001$ .

**FIGURE 6**

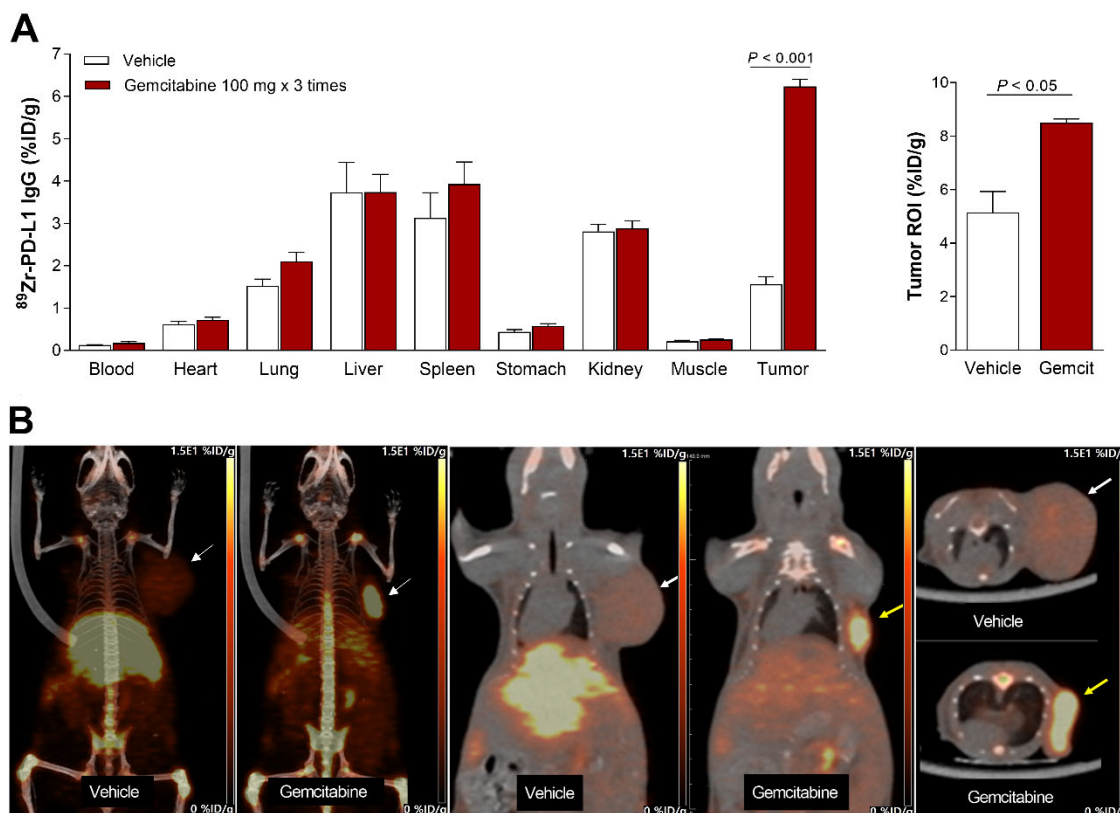


**FIGURE 6.** Effect of gemcitabine on tumor  $^{89}\text{Zr}$ -anti-PD-L1 uptake. (A) Biodistribution in CT26 tumor mice treated with vehicle or gemcitabine at day 7 (left). PET-based tumor activity is shown on the right. Data are mean  $\pm$  S.D. of %ID/g ( $n = 5$  per group). (B) Representative maximum intensity projection (left), coronal (middle), and transaxial (right) PET images of vehicle- and gemcitabine-treated animals.

**FIGURE 7**

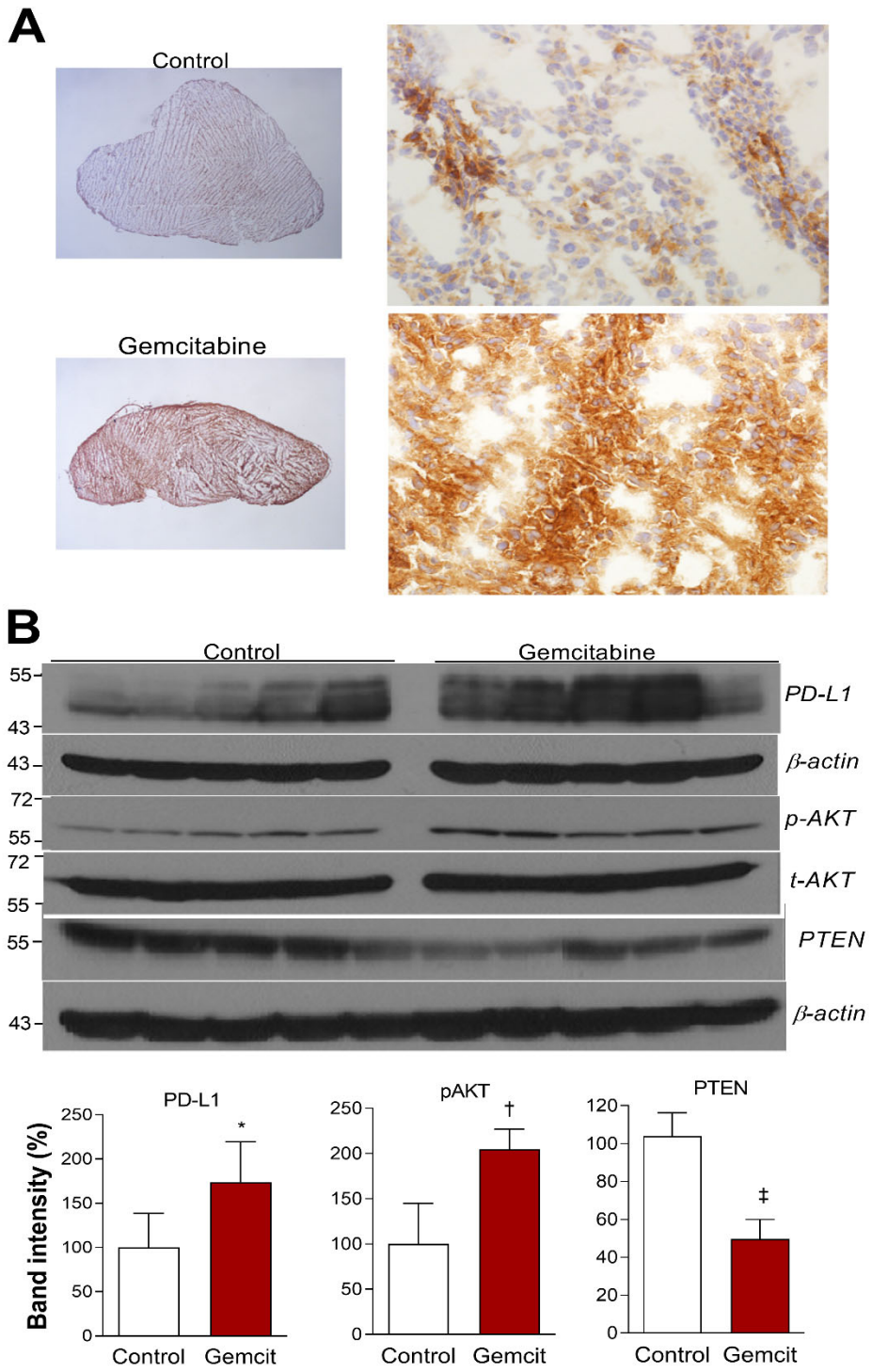


**FIGURE 7.** Effects of gemcitabine on CT26 tumor expression. (A) Representative tumor PD-L1 immunohistochemistry (magnification: left, 12.5×; right, 400×). (B) Immunoblots of tumor tissues (top) and protein band intensities of PD-L1 and PTEN corrected by  $\beta$ -actin and p-AKT corrected by t-AKT (bottom). Bars are mean  $\pm$  S.D. (n = 5 per group). \* $P$  < 0.05, † $P$  < 0.005, ‡ $P$  < 0.001.